The Astronomical Journal, 142:101 (10pp), 2011 October doi:10.1088/0004-6256/142/4/101

FAR-INFRARED AND MOLECULAR CO EMISSION FROM THE HOST GALAXIES OF FAINT QUASARS AT $z \sim 6$

Ran Wang[1,2,11], Jeff Wagg[1,3], Chris L. Carilli[1], Roberto Neri[4], Fabian Walter[5], Alain Omont[6], Dominik A. Riechers[7,12], Frank Bertoldi[8], Karl M. Menten[9], Pierre Cox[3], Michael A. Strauss[10], Xiaohui Fan[2], and Linhua Jiang[2]
[1] National Radio Astronomy Observatory, P.O. Box 0, Socorro, NM 87801, USA
[2] Steward Observatory, University of Arizona, 933 North Cherry Avenue, Tucson, AZ 85721, USA
[3] European Southern Observatory, Alonso de Córdova 3107, Vitacura, Casilla 19001, Santiago 19, Chile
[4] Institute de Radioastronomie Millimetrique, St. Martin d'Heres F-38406, France
[5] Max-Planck-Institute for Astronomy, Königsstuhl 17, 69117 Heidelberg, Germany
[6] Institut d'Astrophysique de Paris, CNRS and Université Pierre et Marie Curie, Paris, France
[7] California Institute of Technology, 1200 East California Boulevard, Pasadena, CA 91125, USA
[8] Argelander-Institut für Astronomie, University of Bonn, Auf dem Hügel 71, 53121 Bonn, Germany
[9] Max-Planck-Institut für Radioastronomie, Auf dem Hügel 71, 53121 Bonn, Germany
[10] Department of Astrophysical Sciences, Princeton University, Princeton, NJ 08544, USA
Received 2011 April 26; accepted 2011 July 17; published 2011 August 23

ABSTRACT

We present new millimeter and radio observations of nine $z \sim 6$ quasars discovered in deep optical and near-infrared surveys. We observed the 250 GHz continuum in eight of the nine objects and detected three of them. New 1.4 GHz radio continuum data have been obtained for four sources, and one has been detected. We searched for molecular CO (6–5) line emission in the three 250 GHz detections and detected two of them. Combined with previous millimeter and radio observations, we study the far-infrared (FIR) and radio emission and quasar-host galaxy evolution with a sample of 18 $z \sim 6$ quasars that are faint at UV and optical wavelengths (rest-frame 1450 Å magnitudes of $m_{1450} \geqslant 20.2$). The average FIR-to-active galactic nucleus (AGN) UV luminosity ratio of this faint quasar sample is about two times higher than that of the bright quasars at $z \sim 6$ ($m_{1450} < 20.2$). A fit to the average FIR and AGN bolometric luminosities of both the UV/optically faint and bright $z \sim 6$ quasars, and the average luminosities of samples of submillimeter/millimeter-observed quasars at $z \sim 2$–5, yields a relationship of $L_{\rm FIR} \sim L_{\rm bol}{}^{0.62}$. Five of the 18 faint $z \sim 6$ quasars have been detected at 250 GHz. These 250 GHz detections, as well as most of the millimeter-detected optically bright $z \sim 6$ quasars, follow a shallower trend of $L_{\rm FIR} \sim L_{\rm bol}{}^{0.45}$ defined by the starburst–AGN systems in local and high-z universe. The millimeter continuum detections in the five objects and molecular CO detections in three of them reveal a few $\times 10^8\ M_\odot$ of FIR-emitting warm dust and $10^{10}\ M_\odot$ of molecular gas in the quasar host galaxies. All these results argue for massive star formation in the quasar host galaxies, with estimated star formation rates of a few hundred $M_\odot\ {\rm yr}^{-1}$. Additionally, the higher FIR-to-AGN luminosity ratio found in these 250 GHz detected faint quasars also suggests a higher ratio between star formation rate and supermassive black hole accretion rate than the UV/optically most luminous quasars at $z \sim 6$.

Key words: galaxies: active – galaxies: high-redshift – galaxies: starburst – molecular data – quasars: general

Online-only material: color figures

1. INTRODUCTION

Understanding the formation and evolution of the first galaxies and the supermassive black holes (SMBHs) they host is a key goal of both observational and theoretical astronomy. The first sample of more than 20 bright quasars at $z \sim 6$ were selected from the imaging data of the Sloan Digital Sky Survey (hereafter SDSS main survey, e.g., Fan et al. 2000, 2006). These objects are very bright in quasar UV and optical emission (SDSS magnitudes of $18.74 \leqslant z_{\rm AB} \leqslant 20.42$) and have SMBHs with masses of $m_{\rm BH} \sim$ a few $10^9\ M_\odot$ (Jiang et al. 2007; Kurk et al. 2007). The dust and molecular gas properties of this bright quasar sample at $z \sim 6$ have been studied at millimeter wavelengths, using the Max Planck Millimeter Bolometer Array (MAMBO), the IRAM Plateau de Bure Interferometer (PdBI), and the Very Large Array (VLA; Bertoldi et al. 2003a, 2003b; Petric et al. 2003; Walter et al. 2003, 2004, 2009; Carilli et al. 2004, 2007; Riechers et al. 2009; Wang et al. 2007, 2008a, 2010). About 30% of them have strong continuum emission at 250 GHz from 40 to 60 K warm dust (Bertoldi et al. 2003a; Petric et al. 2003; Wang et al. 2007, 2008a). The FIR luminosities of the MAMBO detections are a few $\times 10^{12}\ L_\odot$ to $10^{13}\ L_\odot$, and the estimated dust masses are a few $\times 10^8\ M_\odot$ (Beelen et al. 2006; Bertoldi et al. 2003a; Wang et al. 2008b). Most of the 250 GHz detected sources have also been detected in molecular CO line emission with PdBI, yielding molecular gas masses of $(0.7\text{–}3) \times 10^{10}\ M_\odot$ (Walter et al. 2003; Carilli et al. 2007; Riechers et al. 2009; Wang et al. 2010, 2011). The FIR–CO and FIR–radio luminosity ratios of these objects are consistent with the trend defined by dusty starburst systems at low and high redshifts (Riechers et al. 2006; Beelen et al. 2006; Wang et al. 2008a). The results provide direct evidence for massive star formation at a rate of $\sim 10^3\ M_\odot\ {\rm yr}^{-1}$, indicating that bulges are being formed at the same time that the SMBH is rapidly accreting in at least 1/3 of the optically bright quasar systems at $z \sim 6$ (Wang et al. 2008a). Molecular CO (3–2) and (7–6) line emission was resolved in one of the FIR and CO luminous quasars, SDSS J114816.64+525150.3

[11] Jansky Fellow.
[12] Hubble Fellow.

Table 1
Summary of the New Observations

Name	Redshift	m_{1450}	$S_{250\ \mathrm{GHz}}$ (mJy)	$S_{1.4\ \mathrm{GHz}}$ (μJy)	$I\Delta v_{\mathrm{CO(6-5)}}$ (Jy km s^{-1})	FWHM (km s^{-1})	S_{con} (mJy)
(1)	(2)	(3)	(4)	(5)	(6)	(7)	(8)
SDSS J012958.51−003539.7	5.7794 ± 0.0008	22.28	**2.37 ± 0.49**	...	0.37 ± 0.07	283 ± 87	0.14 ± 0.04
SDSS J020332.39+001229.3	5.72	20.97	**1.85 ± 0.46**	**195 ± 22**[a]	<0.32	...	<0.12
SDSS J023930.24−004505.4	5.82	22.28	1.29 ± 0.54	...	...	...	...
ULAS J131911.29+095051.4	6.1321 ± 0.0012	19.65	**4.20 ± 0.65**	**64 ± 17**	0.43 ± 0.09	537 ± 123	0.31 ± 0.08
CFHQS J150941.78−174926.8	6.12	19.82	1.00 ± 0.46[b]	23 ± 18	...	...	...
SDSS J205321.77+004706.8	5.92	21.20	0.09 ± 0.63	...	...	...	...
SDSS J214755.40+010755.0	5.81	21.65	−0.36 ± 0.61	−28 ± 18	...	...	...
SDSS J230735.40+003149.0	5.87	21.73	−0.56 ± 0.53	−21 ± 17	...	...	...
SDSS J235651.58+002333.3	6.00	21.77	0.21 ± 0.49	...	...	...	...

Notes. Column 1: name; Column 2: redshift. CO redshifts are presented for the two sources detected by the PdBI, and we list the redshifts measured with the UV quasar emission lines from the discovery papers for the other six sources (Jiang et al. 2008, 2009); Column 3: rest-frame 1450 Å magnitudes from the discovery papers (Mortlock et al. 2009; Jiang et al. 2008, 2009). Column 4: MAMBO measurements of the 250 GHz dust continuum; Column 5: VLA measurements of the 1.4 GHz radio continuum; Columns 6 and 7: line flux and FWHM of the CO (6–5) line emission; Column 8: measurement of the dust continuum at the CO (6–5) line frequency. The 250 GHz and 1.4 GHz detections are marked as boldface.
[a] Wang et al. (2008a).
[b] Willott et al. (2007).

at $z = 6.42$, revealing a source size of ∼5 kpc (Walter et al. 2004, 2009). The dynamical mass estimated with the size and line width of the CO emission suggest an SMBH spheroidal bulge mass ratio an order of magnitude higher than the typical present-day value (Walter et al. 2004).

$z \sim 6$ quasars that are fainter at UV and optical wavelengths have been discovered from deep optical near infrared surveys (the SDSS southern deep imaging survey, $20.54 \leqslant z_{\mathrm{AB}} \leqslant 22.16$; Jiang et al. 2008, 2009, the Canada–France High-redshift Quasar Survey (CFHQS), $20.26 \leqslant z_{\mathrm{AB}} \leqslant 24.40$; Willott et al. 2007, 2009, 2010a). Near-infrared spectroscopic observations of some of these faint quasars reveal that they are likely to be accreting at the Eddington rate, and have less massive black holes (i.e., 10^8 to $10^9\ M_\odot$) than the SDSS main survey $z \sim 6$ quasar sample (Kurk et al. 2009; Willott et al. 2010b). The steepness of the quasar luminosity function at high redshifts is such that lower-luminosity/mass objects are more common. Thus, these faint $z \sim 6$ quasars provide an important sample to understand SMBH-host galaxy formation at the earliest epoch.

The millimeter dust continuum emission from the faint $z \sim 6$ quasars was first studied with a small sample of four objects discovered by CFHQS (Willott et al. 2007). One of them was detected at 250 GHz with a flux density of ∼1 mJy, indicating a FIR continuum luminosity from dust of $\gtrsim 10^{12}\ L_\odot$. The mean 250 GHz flux density of the four quasars when stacked is ∼0.6 mJy, which is about a factor of two smaller than the average emission of the $z \sim 6$ luminous quasar sample (Willott et al. 2007; Wang et al. 2008a). We subsequently detected 250 GHz dust continuum and molecular CO (6–5) line emission in another two $z \sim 6$ quasars with $z_{\mathrm{AB}} \sim 20.7$ (SDSS J205406.42−000514.8 and NDWFS J142516.30+325409.0, Jiang et al. 2008; Cool et al. 2006; Wang et al. 2008a, 2010) and CO (2–1) line emission from one CFHQS quasar at $z = 6.2$ (CFHQS J142952+544717,[13] Willott et al. 2010a; Wang et al. 2011). These observations revealed a few $10^8\ M_\odot$ of 40-to-60 K warm dust and $10^{10}\ M_\odot$ of molecular gas in the quasar host galaxies, i.e., masses comparable to those found with the bright $z \sim 6$ quasars.

[13] We exclude this object from our analysis throughout this paper as there is no published millimeter continuum flux density for this object.

In this paper, we report new millimeter and radio observations of nine $z \sim 6$ quasars. We then study the FIR and radio emission with a sample of 18 $z \sim 6$ quasars that are faint at UV and optical wavelengths, and investigate the dust and molecular gas emission properties and star-forming activity in the host galaxies of the millimeter-detected objects. We summarize the current quasar sample at $z \sim 6$ and describe the new millimeter and radio observations in Section 2, present the results in Section 3, analyze the continuum emission properties of the faint $z \sim 6$ quasar sample in Section 4, discuss the star formation and quasar-host evolution in Section 5, and conclude in Section 6. A Λ-CDM cosmology with $H_0 = 71\ \mathrm{km\ s^{-1}\ Mpc^{-1}}$, $\Omega_M = 0.27$ and $\Omega_\Lambda = 0.73$ is adopted throughout this paper (Spergel et al. 2007).

2. SAMPLE AND OBSERVATIONS

2.1. Sample

There are 33 $z \sim 6$ quasars that have published millimeter and radio observations from the literature (Bertoldi et al. 2003a; Petric et al. 2003; Carilli et al. 2004; Wang et al. 2007, 2008a; Willott et al. 2007). In this paper, we present new MAMBO observations of the 250 GHz dust continuum emission from eight $z \sim 6$ quasars (Table 1) and molecular CO observations of three of them. Seven of the eight sources were discovered from the SDSS southern survey with optical magnitudes of $20.87 \leqslant z_{\mathrm{AB}} \leqslant 22.16$ (Jiang et al. 2008, 2009), and the other source, ULAS J131911.29+095051.4 (hereafter J1319+0950), was selected from the UKIRT Infrared Deep Sky Survey with $z_{\mathrm{AB}} = 19.99$ (UKIDSS; Mortlock et al. 2009). Seven of the eight objects (all but SDSS J020332.39+001229.3, hereafter J0203+0012) have never been observed at millimeter wavelengths before. We also report new radio 1.4 GHz continuum observations for three of eight new MAMBO-observed objects and another $z \sim 6$ quasar from CFHQS (Willott et al. 2007).

The new observations, together with the previous data, now provide us a sample of forty 250 GHz-observed $z \sim 6$ quasars with optical magnitudes over a wide range, i.e., $18.74 \leqslant z_{\mathrm{AB}} \leqslant 22.16$, or quasar rest-frame 1450 Å AB magnitudes of $18.81 \leqslant m_{1450} \leqslant 22.28$. Wang et al. (2008a) studied the dust emission from quasars at $z \sim 6$, mainly based on the most

Table 2
Previous Observations of the $m_{1450} \geqslant 20.2$ $z \sim 6$ Quasars

Name	Redshift	m_{1450}	$S_{250\,\mathrm{GHz}}$ (mJy)	$S_{1.4\,\mathrm{GHz}}$ (μJy)	L_{FIR}[a] ($10^{12}\,L_{\odot}$)	M_{dust} ($10^{8}\,M_{\odot}$)	M_{gas} ($10^{10}\,M_{\odot}$)	Reference
(1)	(2)	(3)	(4)	(5)	(6)	(7)	(8)	(9)
SDSS J000552.34−000655.8	5.85	20.83	0.36 ± 0.48	40 ± 130	<3.4	...	...	1,2
CFHQS J003311.40−012524.9	6.13	21.78[b]	$\mathbf{1.13 \pm 0.36}$	-27 ± 19	2.6 ± 0.8	1.5	...	2,3
SDSS J030331.40−001912.9	6.08	21.28	0.23 ± 0.51	-85 ± 62	<3.5	...	...	2
SDSS J035349.76+010405.4	6.05	20.22	1.20 ± 0.46	17 ± 19	<3.2	...	...	2
NDWFS J142516.30+325409.0	5.89	20.62[b]	$\mathbf{2.27 \pm 0.51}$	20 ± 20	5.4 ± 1.2	3.0	2.0	2,4
FIRST J142738.59+331242.0	6.12	20.33[b]	0.39 ± 0.66	$\mathbf{1730 \pm 131}$	<4.6	...	...	2,5
SDSS J163033.90+401209.6	6.05	20.64	0.80 ± 0.60	14 ± 15	<4.2	...	...	2,6
CFHQS J164121.64+375520.5	6.05	21.30[b]	0.08 ± 0.46	-30 ± 32	<3.2	...	...	2,3
SDSS J205406.42−000514.8	6.04	20.60	$\mathbf{2.38 \pm 0.53}$	17 ± 23	5.5 ± 1.2	3.1	1.2	2,4
SDSS J231546.36−002357.5	6.12	21.34	0.28 ± 0.60	31 ± 16	<4.1	...	...	2
CFHQS J232908.28−030158.8	6.42	21.65[b]	0.01 ± 0.50	14 ± 22	<3.4	...	...	2

Notes.
[a] The upper limits of L_{FIR} are derived with the 3σ upper limits of the 250 GHz flux densities.
[b] The values are calculated from the absolute 1450 Å magnitudes in the discovery papers (Cool et al. 2006; McGreer et al. 2006; Willott et al. 2007). The 250 GHz and 1.4 GHz detections are marked as boldface.
References. (1) Wang et al. 2007; (2) Wang et al. 2008a; (3) Willott et al. 2007; (4) Wang et al. 2010; (5) McGreer et al. 2006; (6) Bertoldi et al. 2003a.

luminous sample from the SDSS main survey. In this paper, we investigate the FIR and radio emission properties of the fainter quasars at $z \sim 6$, i.e., a subsample of 18 objects with $m_{1450} \geqslant 20.2$ (Tables 1 and 2), and compare them to the bright $z \sim 6$ quasars ($m_{1450} < 20.2$) discussed in previous papers (Bertoldi et al. 2003a; Petric et al. 2003; Wang et al. 2008a). We will discuss the optical measurements and quasar UV and bolometric luminosities based on m_{1450}, which is derived from the SDSS z-band magnitudes and deep optical spectra (e.g., Fan et al. 2000, 2001, 2003, 2004, 2006; Jiang et al. 2008, 2009; Willott et al. 2007), or from infrared photometry in the cases in which significant dust reddening is presented in the optical spectra (e.g., McGreer et al. 2006).

2.2. Observations

Observations of the 250 GHz dust continuum from the eight $z \sim 6$ quasars were carried out using the MAMBO-II 117 element array on the IRAM 30 m telescope (Kreysa et al. 1998) in the winters of 2008–2009 and 2009–2010. We adopted the standard on–off photometry mode with a chopping rate of 2 Hz by 32″ in azimuth (see also Wang et al. 2007, 2008a). The on-source observing time was about 1–3 hr for each object, to achieve 1σ rms sensitivities of ∼0.5–0.7 mJy. We used the MOPSIC pipeline (Zylka 1998) to reduce the data, and three sources, J1319+0950, SDSS J012958.51−003539.7 (hereafter J0129−0035), and J0203+0012, were detected at $\geqslant 4\sigma$. Wang et al. (2008a) observed J0203+0012 with MAMBO and did not detect the source with a 1σ rms of 0.7 mJy. Our new observations, together with the old data, improve the rms to 0.46 mJy for this object, and we detect the 250 GHz continuum at 4σ. We have also obtained a 2.4σ signal from another source, SDSS J023930.24−004505.4 (hereafter J0239−0045).

We also observed four $z \sim 6$ quasars at 1.4 GHz in Winter 2008–2009, using the VLA in A configuration with a synthesized beam size of FWHM ∼ 1.″4. Flux scales were measured using the standard VLA calibrators of 3C286 and 3C48, and phase calibrations were performed every 30 minutes on nearby phase calibrators (1254−116, 1507−168, 2136+006, and 2323−032). The typical rms noise level was ∼17 μJy beam^{-1} in three hr of observing time for each source. We reduced the data with the standard VLA wide field data reduction software AIPS, and one source, J1319+0950, was detected at $\sim 3.8\sigma$.

We searched for molecular CO (6–5) line emission from the three MAMBO detections using the 3 mm receiver on the PdBI. The source J1319+0950 was observed in 2009 Summer in C and D configurations (i.e., a spatial resolution of FWHM ∼ 3.″5) with the narrowband correlator, which provides a bandwidth of 1 GHz in dual polarization. The observations of J0129−0035 and J0203+0012 were carried out using the new wide band correlator WideX with a bandwidth of 3.6 GHz in dual polarization, which covers well the Lyα-redshift uncertainty of $\Delta z \sim \pm 0.03$ (Jiang et al. 2009). The observations were performed in 2010 Summer in D configuration with a synthesized beam size of FWHM ∼ 5″. Phase calibration was performed every 20 minutes with observations of phase calibrators, 1307+121 and 0106+013, and we observed MWC 349 as the flux calibrator. We reduced the data with the IRAM GILDAS software package (Guilloteau & Lucas 2000). The CO (6–5) line emission is detected from J1319+0950 at 4.8σ in 10.3 hr of on-source time with an rms sensitivity of 0.50 mJy beam^{-1} per 70 km s^{-1} binned channel, and from J0129−0035 at 5.3σ in 8.8 hr with an rms of 0.55 mJy beam^{-1} per 100 km s^{-1} channel. We also detect the continuum at $> 3\sigma$ at the CO (6–5) line frequency in both objects. The other source, J0203+0012, was undetected in both CO and 3 mm continuum in 13.9 hr of on-source time, with a sensitivity of 0.44 mJy beam^{-1} per 100 km s^{-1} channel.

3. RESULTS

3.1. Notes for Individual Objects

We summarize the new millimeter and radio observations of the nine $z \sim 6$ quasars in Table 1. Detailed measurements of the three new 250 GHz dust continuum/molecular CO (6–5) detections are listed below.

J1319+0950. The source was discovered in UKIDSS with $m_{1450} = 19.65$, which lies in the typical magnitude range of the optically bright $z \sim 6$ quasars selected from the SDSS main survey (Mortlock et al. 2009). We detect the 250 GHz dust continuum emission from this object with a flux density of $S_{250\,\mathrm{GHz}} = 4.20 \pm 0.65$ mJy, which is the third-strongest 250 GHz detection among the known $z \sim 6$

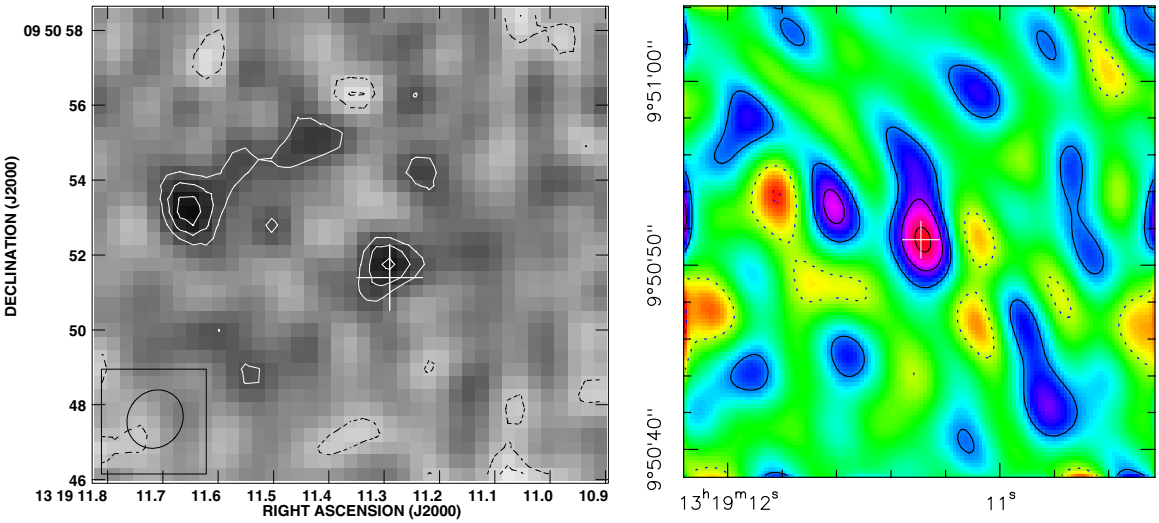

Figure 1. Left: VLA 1.4 GHz continuum image of the $z = 6.132$ quasar J1319+0950. The beam size is $1\farcs61 \times 1\farcs45$, which is plotted on the bottom left, and the contour levels are $(-3, -2, 2, 3, 4) \times 15\ \mu$Jy beam^{-1}. Right: PdBI 97 GHz continuum image of the quasar averaged over the line-free channels. The synthesized beam size (FWHM) is $3\farcs5$, and the contour levels are $(-2, -1, 1, 2, 3) \times 0.08$ mJy beam^{-1}. The cross in both plots denotes the optical position of the quasar (Mortlock et al. 2009).

(A color version of this figure is available in the online journal.)

quasars. The 1.4 GHz radio continuum is also detected from our VLA observation, with $S_{1.4\,\mathrm{GHz}} = 64 \pm 17\ \mu$Jy (left panel of Figure 1). The radio emission appears unresolved with a peak at $13^{\mathrm{h}}19^{\mathrm{m}}11\fs30$, $09^\circ50'51\farcs8$, i.e., within $0\farcs4$ of the optical quasar position. We also see a 4σ peak ($S_{1.4\,\mathrm{GHz}} = 68 \pm 17\ \mu$Jy) at $13^{\mathrm{h}}19^{\mathrm{m}}11\fs65$, $09^\circ50'53\farcs2$ on the radio map, which is $5\farcs6$ away from the quasar. For comparison, only 0.02 detections with $S_{1.4\,\mathrm{GHz}} \geqslant 60\ \mu$Jy are expected from a random circular sky area with a radius of $6''$, according to the 1.4 GHz radio source counts from previous deep VLA observations (i.e., $N(> S_{1.4\,\mathrm{GHz}}) = (0.40 \pm 0.04)(S_{1.4\,\mathrm{GHz}}/75\ \mu\mathrm{Jy})^{(-1.43\pm0.13)}$; Fomalont et al. 2006). No optical counterpart has been found at the radio source position in the NASA/IPAC Extragalactic Database or the SDSS images.

We observed the CO (6–5) line emission from this object with the PdBI. The line is detected at 4.8σ on the velocity-integrated map with a line flux of 0.43 ± 0.09 Jy km s^{-1}, $0\farcs9$ away from (i.e., consistent with) the quasar position (the upper panel of Figure 2). A Gaussian fit to the line spectrum yields a peak line flux density of 0.80 ± 0.15 mJy beam^{-1} and a line width of FWHM $= 537 \pm 123$ km s^{-1}, centered at the redshift of $z = 6.1321 \pm 0.0012$. This is slightly higher than, but consistent with the Mg II redshift of $z = 6.127 \pm 0.007$, considering the measurement errors (±0.004; Mortlock et al. 2009) and the typical velocity shift and scatters 97 ± 269 km s^{-1} (-0.002 ± 0.006 in redshift) between the broad Mg II line emission and the quasar systemic redshift (Richards et al. 2002). We also detect the continuum under the CO (6–5) line emission with a peak value of $S_{97\,\mathrm{GHz}} = 0.31 \pm 0.08$ mJy beam^{-1} on the continuum map averaged over the line-free channels (right panel of Figure 1). We adopt this as the continuum flux density as the source is unresolved with the $5''$ beam. We checked the position of the 1.4 GHz radio source $5\farcs6$ away from the quasar in the PdBI CO/97 GHz continuum images. There is no clear ($\geqslant 3\sigma$) detection at this position and the measurement in the 97 GHz continuum image is 0.19 ± 0.08 mJy (right panel of Figure 1).

J0129−0035. This is the faintest of the SDSS $z \sim 6$ quasars, with $m_{1450} = 22.16$ (Jiang et al. 2009). We detect 250 GHz dust continuum from the quasar host galaxy, with a flux density of $S_{250\,\mathrm{GHz}} = 2.37 \pm 0.49$ mJy, comparable to the flux densities of the optically bright $z \sim 6$ quasars with 250 GHz detections.

We detected the CO (6–5) line in this source with a flux of 0.37 ± 0.07 Jy km s^{-1}, i.e., at 5.3σ, integrated over a velocity range of 380 km s^{-1} (the middle panel of Figure 2). The line width fitted with a single Gaussian is 283 ± 87 km s^{-1}, with a line peak of 1.2 ± 0.3 mJy. The host galaxy redshift measured with the CO line is $z = 5.7794 \pm 0.0008$, which is in good agreement with the optical redshift of $z_{\mathrm{Ly}\alpha} = 5.78 \pm 0.03$ measured with Lyα (Jiang et al. 2009). The underlying dust continuum is also detected with a flux density of $S_{102\,\mathrm{GHz}} = 0.14 \pm 0.04$ mJy.

J0203+0012. This object is a broad absorption line quasar discovered by both the SDSS southern survey (Jiang et al. 2008) and the UKIDSS survey (Venemans et al. 2007; Mortlock et al. 2009) with $m_{1450} = 20.97$. The redshift measured with the quasar N V line emission is $z = 5.72$ (Mortlock et al. 2009). Wang et al. (2008) detected the 1.4 GHz radio continuum with $S_{1.4\,\mathrm{GHz}} = 195 \pm 22\ \mu$Jy (Wang et al. 2008). Our MAMBO observation yields a 250 GHz dust continuum flux density of $S_{250\,\mathrm{GHz}} = 1.85 \pm 0.46$ mJy. We have searched for the CO (6–5) line emission from this object over a wide redshift range, from $z = 5.60$ to 5.84, but did not detect it in 14 hr of on-source time. Assuming a line width of 600 km s^{-1}, the 3σ upper limit of the CO flux is estimated to be 0.32 Jy km s^{-1} (the lower panel of Figure 2).[14] The dust continuum at the CO (6–5) line frequency is also undetected with a continuum sensitivity of 0.04 mJy beam^{-1} and a 3σ upper limit of 0.12 mJy.

3.2. FIR and Radio Luminosities and Dust Mass

We calculate the FIR luminosities and upper limits for the eight $z \sim 6$ quasars observed by MAMBO. We model the FIR emission with an optically thin graybody and normalize the model to the MAMBO-250 GHz and available PdBI 3 mm

[14] We estimate the 3σ upper limit for the CO line flux as $3\sigma_{\mathrm{channel}}(\Delta V_{\mathrm{line}}\Delta V_{\mathrm{channel}})^{1/2}$, where ΔV_{line} is the assumed line width, and $\sigma_{\mathrm{channel}}$ and $\Delta V_{\mathrm{channel}}$ are the rms per channel and channel width listed in Section 2.2 (Seaquist et al. 1995).

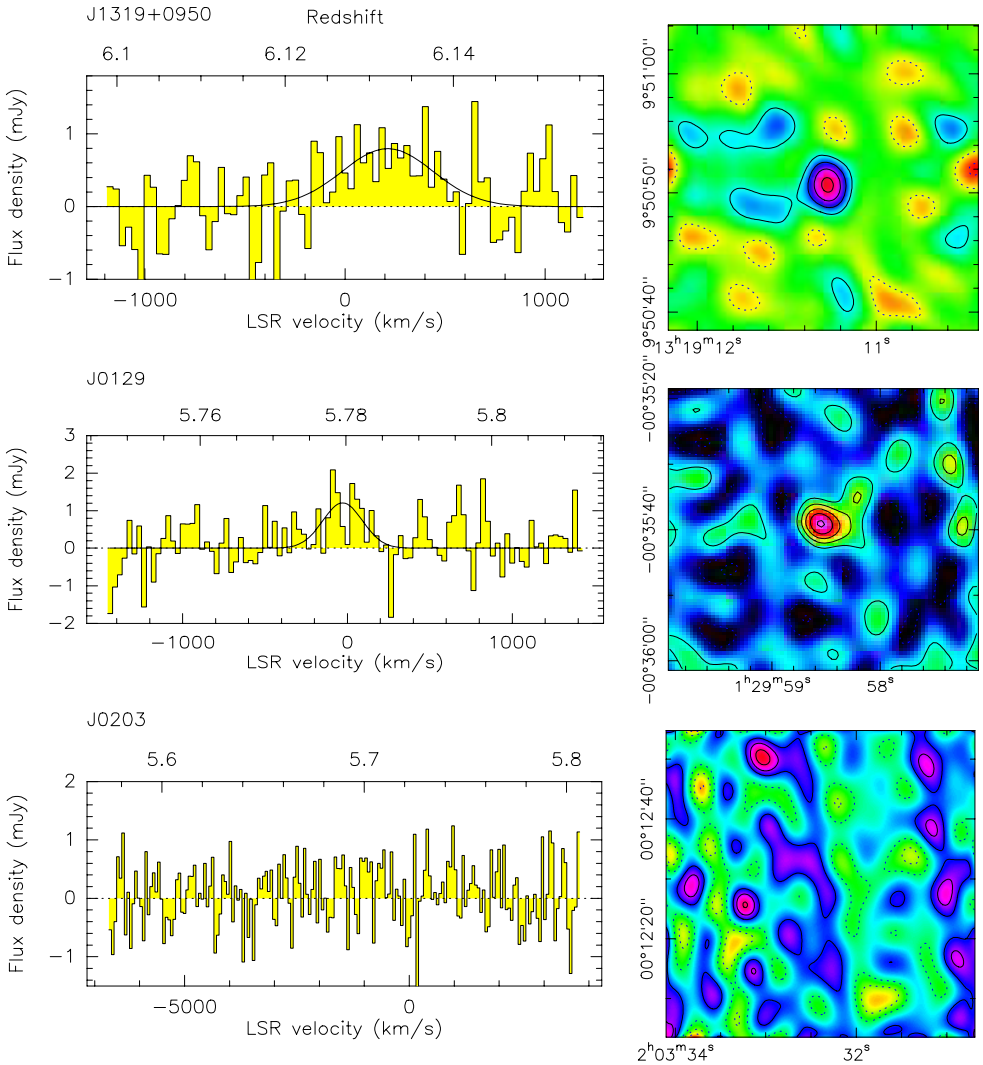

Figure 2. CO line spectra (left) and velocity-integrated images (right) of the three $z \sim 6$ quasars observed with the PdBI. The continuum emission underlying the CO spectra is removed for the two detections, J1319+0950 and J0129−0035. The synthesized beam size (FWHM) of the CO velocity-integrated image of J1319+0950 is $\sim 3\farcs5$, and $\sim 5''$ for J0129−0035 and J0203+0012. The top abscissae of the CO spectra give the redshift range of the spectral windows, and zero velocity in each panel corresponds to the optical/near-infrared redshifts of $z = 6.127$, 5.780, 5.720 from the discovery papers (Mortlock et al. 2009; Jiang et al. 2009). The solid lines in the spectra show Gaussian fits to the line emission. The CO peak positions are consistent with the optical quasars for the two detections.

(A color version of this figure is available in the online journal.)

dust continuum flux densities/3σ upper limits (see also Wang et al. 2007, 2008). A dust temperature of $T_d = 47$ K and emissivity index of $\beta = 1.6$ are adopted in the model; these are typical values for the FIR and CO luminous quasars at lower redshifts (Beelen et al. 2006). We then integrate the model FIR SED from 42.5 μm to 122.5 μm to calculate the total FIR luminosities/upper limits. The FIR luminosity of the strongest MAMBO detection, J1319+0950, is $1.0 \times 10^{13}\,L_\odot$, making it one of the most FIR-luminous objects among the $z \sim 6$ quasar sample. The other two MAMBO-detected objects are from the SDSS southern survey sample and have FIR luminosities of $4 \sim 5 \times 10^{12}\,L_\odot$. We also estimate the dust masses for the three MAMBO detections, using $M_{\rm dust} = L_{\rm FIR}/4\pi \int \kappa_\nu B_\nu d\nu$, where B_ν is the Planck function and $\kappa_\nu = \kappa_0(\nu/\nu_0)^\beta$ is the dust absorption coefficient with $\kappa_0 = 18.75\,{\rm cm^2\,g^{-1}}$ at 125 μm (Hildebrand 1983). The estimated dust masses of the three sources are $(2.5\text{–}5.7) \times 10^8\,M_\odot$. We finally calculate the 1.4 GHz radio continuum luminosity densities and upper limits for the four VLA observed objects. We assume a power-law continuum of $f_\nu \sim \nu^{-0.75}$ (Condon 1992) to correct the observed frequency to the quasar rest frame. The results are summarized in Table 3; we also include the 1.4 GHz radio luminosity of J0203+0012 from Wang et al. (2008a).

3.3. CO Luminosities and Molecular Gas Masses

We calculate the CO (6–5) line luminosities and upper limits for the three CO-observed $z \sim 6$ quasars, using $L'_{\rm CO(6-5)} = 3.25 \times 10^7 I\Delta v_{\rm CO(6-5)} {\nu_{\rm obs}}^{-2} {D_L}^2 (1+z)^{-3}$ (K km s^{-1} pc^2), where $I\Delta v_{\rm CO(6-5)}$ is the line flux or 3σ upper limit in Jy km s^{-1} presented in Table 1, $\nu_{\rm obs}$ is the observed frequency of the CO (6–5) line in GHz, D_L is the luminosity distance in Mpc, and z is the quasar redshift (Solomon & Vanden Bout 2005). We then assume a CO excitation ladder similar to that of J1148+5251 (Riechers et al. 2009), for which $L'_{\rm CO(6-5)}/L'_{\rm CO(1-0)} \approx 0.78$, allowing us to calculate the CO (1–0) luminosities. The FIR-to-CO(1–0) luminosity ratios of J1319+0950 and J0129−0035 are 520 and 340 $L_\odot\,{\rm K^{-1}\,km\,s^{-1}\,pc^2}$, respectively, which are similar to the values found for other $z \sim 6$ CO-detected quasars (Wang et al. 2010). We then calculate the molecular gas masses

Table 3
Derived Parameters for the New Observations

Name	$L_{\rm FIR}$ ($10^{12}\,L_\odot$)	$M_{\rm dust}$ ($10^8\,M_\odot$)	$L_{1.4\,\rm GHz}$ ($L_\odot\,{\rm Hz}^{-1}$)	$L'_{\rm CO(6-5)}$ ($10^{10}\,{\rm K\,km\,s^{-1}\,pc^2}$)	$L'_{\rm CO(1-0)}$ ($10^{10}\,{\rm K\,km\,s^{-1}\,pc^2}$)	$M_{\rm gas}$ ($10^{10}\,M_\odot$)
(1)	(2)	(3)	(4)	(5)	(6)	(7)
J0129−0035	5.2 ± 0.9	2.9	...	1.2 ± 0.2	1.5 ± 0.3	1.2
J0203+0012	4.4 ± 1.1	2.5	0.118 ± 0.013	<1.0	<1.3	<1.0
J0239−0045	<3.9	...	...	...	...	...
J1319+0950	10.0 ± 1.3	5.7	0.045 ± 0.012	1.5 ± 0.3	1.9 ± 0.4	1.5
J1509−1749	<3.2	...	<0.038	...	...	...
J2053+0047	<4.4	...	...	...	...	...
J2147+0107	<4.4	...	<0.034	...	...	...
J2307+0031	<3.8	...	<0.032	...	...	...
J2356+0023	<2.8	...	...	...	...	...

($M_{\rm gas} = M[{\rm H_2 + He}]$), adopting a CO luminosity-to-gas mass conversion factor of $\alpha = 0.8\,M_\odot\,({\rm K\,km\,s^{-1}\,pc^2})^{-1}$ seen in low-redshift ultra-luminous infrared galaxies (ULIRGs; Solomon et al. 1997; Downes & Solomon 1998). The molecular gas masses for the two new CO detections are all of order $10^{10}\,M_\odot$ (Table 3).

4. ANALYSIS

The new observations increase the sample of MAMBO-observed $z \sim 6$ quasars to 40 objects (Bertoldi et al. 2003a; Petric et al. 2003; Willott et al. 2007; Wang et al. 2007, 2008a). In this paper, we study their FIR and radio emission properties, focusing on the 18 sources that are fainter at UV and optical wavelengths ($20.20 < m_{1450} \leqslant 22.28$, hereafter faint $z \sim 6$ quasars) and compare them with the first sample of millimeter-studied $z \sim 6$ quasars from the SDSS main survey (hereafter bright $z \sim 6$ quasars; Bertoldi et al. 2003a; Petric et al. 2003; Wang et al. 2007, 2008a). The MAMBO observations of these faint $z \sim 6$ quasars have typical sensitivities (0.4–0.6 mJy) comparable to or slightly lower than that achieved in previous MAMBO observations of the SDSS main survey $z \sim 6$ quasars (0.5–1.1 mJy; Petric et al. 2003; Wang et al. 2007, 2008) and the optically bright quasar samples at redshifts 2 and 4 (Omont et al. 2001, 2003; Carilli et al. 2001). Five of the 18 sources are detected at 250 GHz at $\geqslant 3\sigma$ (Wang et al. 2007, 2008a; Willott et al. 2007), yielding a detection rate of $28\% \pm 12\%$, or $25\% \pm 14\%$ if we consider the subsample of 12 objects from the SDSS southern survey selected with the same color selection criteria (three detections; Fan et al. 2004; Jiang et al. 2008; 2009; Wang et al. 2008a; this work). These are slightly lower than the MAMBO detection rate of $\gtrsim$30% found with the optically bright quasar samples from $z = 2$ to 6 (Omont et al. 2001, 2003; Carilli et al. 2001; Wang et al. 2008a), but are consistent within the errors.

We searched for molecular CO (6–5) line emission in four of the five MAMBO-detected faint $z \sim 6$ quasars, and detected three (Wang et al. 2010), indicating that highly excited molecular gas is ubiquitous in these millimeter (FIR) luminous quasar–galaxy systems at the earliest epoch. Fourteen of the 18 sources have radio 1.4 GHz continuum observations with typical 1σ rms of $\sim 20\,\mu$Jy, and only two of them, J0203+0012 and J1427+3312,[15] have radio detections (McGreer et al. 2006; Wang et al. 2007, 2008a; this work). This gives a much lower radio detection rate for the faint $z \sim 6$ quasar sample than that of the bright objects; nine out of 22 $z \sim 6$ quasars with $m_{1450} < 20.2$ were detected at 1.4 GHz with similar observational sensitivities ($\sim 20\,\mu$Jy; Petric et al. 2003; Carilli et al. 2004; Wang et al. 2007, 2008a). The 1.4 GHz continuum flux density is 1.7 mJy for J1427+3312 (McGreer et al. 2006) and 195 μJy for J0203+0012 (Wang et al. 2008a), indicating radio-loud nuclei in the two objects[16] (Momjian et al. 2008). Deep observations are required to better constrain the radio emission from the radio-quiet UV/optical faint $z \sim 6$ quasars.

4.1. The Average FIR and Radio Emission

We calculate the average 250 GHz and 1.4 GHz continuum for the 18 faint $z \sim 6$ quasars. The mean flux densities are derived for (1) all sources, (2) MAMBO detections, and (3) MAMBO non-detections, using the MAMBO and VLA measurements weighted by inverse variance (see also Wang et al. 2008a). We also present the average values for the 22 bright quasars ($m_{1450} < 20.2$) for comparison. The average emission of this bright quasar sample is consistent with the results presented in Wang et al. (2008a). We list all the results in Table 4.

The mean 250 GHz flux density is 0.85 ± 0.12 mJy for all 18 faint quasars, and 1.85 ± 0.20 mJy for the five MAMBO-detected sources, which are about 50% and 70% of the values found for the bright quasars, respectively. The results are about the same when the two radio-loud quasars are excluded. The stacking measurement for the 13 MAMBO-undetected sources in the faint sample is 0.33 ± 0.15 mJy, which places an upper limit of <0.78 mJy (stacking average plus the 3σ rms) for the average millimeter dust continuum emission.

We convert the average 250 GHz flux densities to 42.5–122.5 μm FIR luminosities, adopting the assumptions described in Section 3.2, and calculate the average FIR-to-1450 Å luminosity ratios ($\langle L_{\rm FIR}\rangle$ / $\langle L_{1450}\rangle$) for each sample (see Table 4). The average luminosity ratios for all the sources and the MAMBO detections in the faint-quasar sample are two and three times higher than the corresponding values found with bright quasars. This is consistent with the nonlinear FIR-to-active galactic nucleus (AGN) luminosity relationships of $L_{\rm FIR} \sim L_{\rm AGN}^{\alpha}$, where $\alpha < 1$ found with the AGN starburst at low and high redshifts (Beelen 2004; Hao et al. 2005, 2008; Wang et al. 2008a; Serjeant & Hatziminaoglou 2009; Lutz et al. 2010), as we will discuss further in Section 4.2. However, the different average luminosity ratios found with the MAMBO detections in the bright and faint quasar samples may be partly due

[15] Note that J1427+3312 was selected from radio data (McGreer et al. 2006).

[16] The radio-loud quasars are defined as quasars with radio-to-optical flux density ratios of $f_{\nu,5\,\rm GHz}/f_{\nu,4400\,\text{Å}} \geqslant 10$ (Kellermann et al. 1989) where fluxes are measured in the rest frame. We adopt this definition and calculate R assuming a power-law UV-to-optical continuum of $f_\nu \sim \nu^{-0.5}$ (Fan et al. 2000) and radio continuum of $f_\nu \sim \nu^{-0.75}$ (Condon 1992).

Table 4
Average FIR and Radio Emission of the $z \sim 6$ Quasars

Group	Number[a]	$\langle L_{1450}\rangle$[b] ($10^{12}\,L_\odot$)	$\langle f_{250\,\mathrm{GHz}}\rangle$ (mJy)	$\langle L_{\mathrm{FIR}}\rangle$ ($10^{12}\,L_\odot$)	$\frac{\langle L_{\mathrm{FIR}}\rangle}{\langle L_{1450}\rangle}$	Number[c]	$\langle f_{1.4\,\mathrm{GHz}}\rangle$ (μJy)	$\langle L_{1.4\,\mathrm{GHz}}\rangle$[d] ($L_\odot\,\mathrm{Hz}^{-1}$)	q
(1)	(2)	(3)	(4)	(5)	(6)	(7)	(8)	(9)	(10)
Optically faint $z \sim 6$ quasars with $m_{1450} \geqslant 20.2$									
All objects	18	4.3	0.85 ± 0.12	2.0 ± 0.3	0.46	14	19 ± 6	0.012 ± 0.003	1.63 ± 0.15
(radio quiet)	16	4.0	0.79 ± 0.13	1.9 ± 0.3	0.46	12	2 ± 6	<0.013	>1.57
250 GHz detections	5	4.3	1.85 ± 0.20	4.3 ± 0.5	1.01	4	45 ± 10	0.030 ± 0.07	1.59 ± 0.11
(radio quiet)	4	4.2	1.86 ± 0.23	4.3 ± 0.5	1.03	3	1 ± 12	<0.024	>1.68
250 GHz non-detections	13	4.3	0.33 ± 0.15	<1.8	<0.42	10	7 ± 7	<0.019	...
(radio quiet)	12	3.9	0.32 ± 0.15	<1.8	<0.46	9	2 ± 7	<0.015	...
Optically bright $z \sim 6$ quasars with $m_{1450} < 20.2$									
All objects	22	17.6	1.64 ± 0.13	3.8 ± 0.3	0.22	22	50 ± 3	0.033 ± 0.002	1.49 ± 0.04
(radio quiet)	21	16.9	1.68 ± 0.13	3.9 ± 0.3	0.23	21	38 ± 3	0.026 ± 0.002	1.61 ± 0.05
250 GHz detections	8	19.1	2.71 ± 0.18	6.3 ± 0.4	0.33	8	43 ± 4	0.029 ± 0.003	1.77 ± 0.05
250 GHz non-detections	14	16.8	0.55 ± 0.18	1.3 ± 0.4	0.08	14	59 ± 5	0.040 ± 0.003	0.94 ± 0.15
(radio quiet)	13	15.5	0.58 ± 0.18	1.4 ± 0.4	0.09	13	32 ± 5	0.021 ± 0.003	1.23 ± 0.15

Notes. We calculate the average flux densities using $\langle f_\nu\rangle = \sum w_i f_{\nu,i} / \sum w_i$, $w_i = 1/\sigma_{\nu,i}^2$, and $\langle \sigma_\nu\rangle = (\sum w_i)^{-0.5}$ (Omont et al. 2003), where $f_{\nu,i}$ and $\sigma_{\nu,i}$ are the measurement and 1σ rms for each object at 250 GHz or 1.4 GHz. For results with $\langle f_\nu\rangle$ less than $3\langle\sigma_\nu\rangle$, we take the stacking average value plus $3\langle\sigma_\nu\rangle$ as the upper limits of the average flux densities and calculate the corresponding upper limits for the luminosities.

[a] Number of sources observed at 250 GHz.

[b] Average luminosity at rest-frame 1450 Å, derived from m_{1450}.

[c] Number of sources observed at 1.4 GHz.

[d] A radio spectral index of -0.75 (Condon 1992) is adopted here to calculate the rest frame 1.4 GHz lunimosity.

to the selection effect that the detection limit of the MAMBO observations is about the same for the two samples, while the AGN luminosities are different by design.

The average 1.4 GHz continuum flux density, derived from 14 VLA-observed sources in the faint quasar sample, is $19 \pm 6\,\mu$Jy, and $2 \pm 6\,\mu$Jy when the two radio-loud sources are excluded. This suggests an upper limit of $20\,\mu$Jy for the radio-quiet and UV/optically faint $z \sim 6$ quasars. We estimate the average rest-frame 1.4 GHz luminosities/upper limits for the two samples and list the results in Table 4. We plot L_{FIR} versus $L_{\nu,1.4\,\mathrm{GHz}}$ of all the MAMBO-detected $z \sim 6$ quasars together with the average luminosities of the MAMBO-detections and non-detections in Figure 3, and compare them to sample of IRAS-selected local star-forming galaxies (Yun et al. 2001). The local star-forming galaxies with FIR and radio emission powered by the active star formation have an average luminosity ratio of $q = \log(L_{\mathrm{FIR}}/3.75 \times 10^{12}\,L_\odot) - \log(L_{1.4\,\mathrm{GHz}}/L_\odot \cdot \mathrm{Hz}^{-1}) = 2.34$. The range $1.6 < q < 3.0$ contains 98% of the IRAS galaxies (Yun et al. 2001). The average luminosities/upper limits of the MAMBO-detected $z \sim 6$ quasars, though lower than the mean value of $q = 2.34$, are all within this range defined by local star forming galaxies. This argues that, in addition to the AGN power, star formation also contributes significantly to the FIR-to-radio emission of the MAMBO-detected $z \sim 6$ quasars. The average ratio of the MAMBO-undetected bright $z \sim 6$ quasars is offset from this range.

4.2. The FIR-to-AGN Luminosity Relationship

The correlations between FIR luminosities and AGN UV, optical, and bolometric luminosities have been studied widely with samples of infrared and optically selected quasars to understand the origin of quasar FIR emission. Study of samples of the Palomar-Green quasars and Seyfert galaxies shows a relationship of $L_{\mathrm{FIR}} \sim L_{\mathrm{AGN}}^{0.7\sim0.8}$ for typical optically-selected AGN/quasars in the local universe (Hao et al. 2005; Netzer et al. 2007; Lutz et al. 2010). A shallower relationship of $L_{\mathrm{FIR}} \sim L_{\mathrm{AGN}}^{0.4}$ was found for the local IR-luminous quasars hosted by starburst ULIRGs (Hao et al. 2005) and high-redshift FIR-and-CO luminous quasars (Beelen 2004; Hao et al. 2008; Wang et al. 2007; Lutz et al. 2010), which suggests excess FIR emission powered by extreme starburst in these systems. Wang et al. (2008a) reported that the millimeter-detected bright $z \sim 6$ quasars follow the shallow luminosity trend defined by the local IR quasars.

In this work, we investigate the FIR-to-AGN luminosity correlation of the full sample $z \sim 6$ quasars, and compare with the samples of MAMBO-250 GHz or SCUBA-350 GHz observed optically bright quasars at $z \sim 2$–5 (Omont et al. 2001, 2003; Carilli et al. 2001; Priddey et al. 2003a), and local IR quasars (Zheng et al. 2002; Hao et al. 2005). We convert the UV or optical luminosities of all objects to AGN bolometric luminosities assuming a UV-to-optical power-law continuum of $f_\nu \sim \nu^{-0.5}$, and an optical-to-AGN bolometric luminosity conversion factor of $L_{\mathrm{bol}} = 10.4\,\nu L_{\nu,4400\,\text{Å}}$ (Richards et al. 2006). In Figure 4, we plot all the $z \sim 6$ quasars, as well as the local IR quasar sample and the average luminosities of the submillimeter/millimeter ((sub)mm)-observed $z \sim 2$–5 quasar samples (Omont et al. 2003; Hao et al. 2008). The average FIR luminosities of the $z \sim 2$–5 quasars are derived with the mean flux densities at 250 GHz or 350 GHz (Omont et al. 2001, 2003; Carilli et al. 2001; Priddey et al. 2003a), adopting the same assumptions of dust temperature and emissivity index used for the $z \sim 6$ quasars (see Section 3.2). We fit a line to the average luminosities of all these (sub)mm-observed quasar samples at $z \sim 2$ to 6 using the Ordinary Least Square method (Isobe et al. 1990). This yields an relationship of

$$\log\left(\frac{L_{\mathrm{FIR}}}{L_\odot}\right) = (0.62 \pm 0.09)\log\left(\frac{L_{\mathrm{bol}}}{L_\odot}\right) + (3.90 \pm 1.29) \quad (1)$$

between the average FIR and AGN emission in these high-redshift optically selected quasars, and the nonlinear slope of

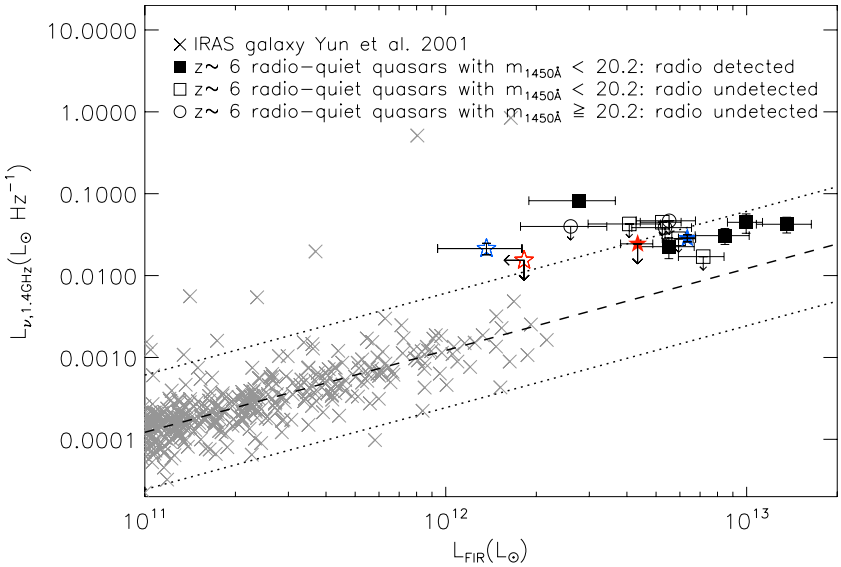

Figure 3. FIR vs. radio luminosity plot of the MAMBO-detected radio-quiet $z \sim 6$ quasars that have radio 1.4 GHz continuum observations. The filled blue and red stars are the average values for the MAMBO-detected optically bright ($m_{1450} < 20.2$) and faint ($m_{1450} \geqslant 20.2$) $z \sim 6$ quasars, respectively. The open stars represent the stacking average or upper limits of the non-detections in the two samples. Only the radio-quiet objects in the $z \sim 6$ quasar samples are plotted here. The crosses are a sample of IRAS star-forming galaxies from Yun et al. (2001). The dashed line shows the average radio–FIR correlation in star-forming galaxies ($q = \log(L_{\rm FIR}/3.75 \times 10^{12}\, L_\odot) - \log(L_{1.4\,\rm GHz}/L_\odot \cdot {\rm Hz}^{-1}) = 2.34$; Yun et al. 2001). The dotted lines represents q values five times higher and lower, which includes 98% of the IRAS galaxies.

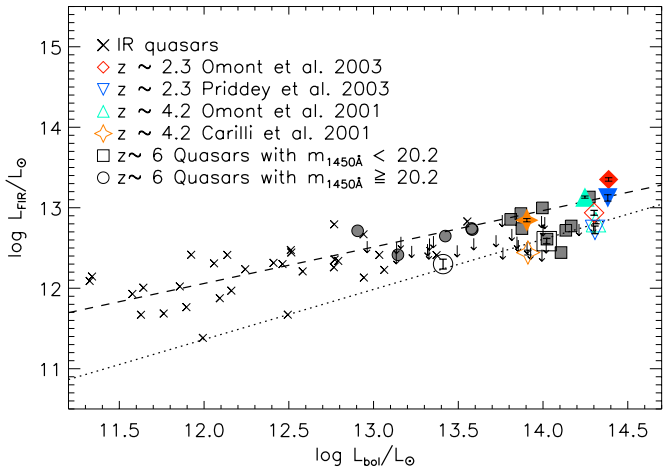

Figure 4. FIR and AGN bolometric luminosity correlations of the $z \sim 6$ quasars, together with samples of local optically selected IR luminous quasars hosted by ULIRGs (Hao et al. 2005; Zheng et al. 2002) and the average luminosities of the (sub)mm-observed quasars at redshift $z \sim 2$–5 (Omont et al. 2001, 2003; Priddey et al. 2003a; Carilli et al. 2001). The filled squares and circles are the MAMBO detections in the bright ($m_{1450} < 20.2$) and faint ($m_{1450} \geqslant 20.2$) $z \sim 6$ quasar samples, respectively, and the arrows indicate 3σ upper limits of the non-detections (see Section 3.2). The $z = 6.0$ quasar, SDSS J130608.26+035626.3, was not detected at 250 GHz (Wang et al. 2007), but was detected by SCUBA at 350 GHz (Priddey et al. 2003b). We estimate the FIR luminosity of this object with the SCUBA flux density and plot it as filled squares. The filled triangles and diamonds are the mean FIR luminosities for the (sub)mm detections in each sample, derived by averaging flux densities at 250 GHz or 350 GHz. The open symbols represent the mean luminosities averaged with both the millimeter detections and non-detections in each sample. The dotted line is a fit to the average luminosities (open symbols) of all the high-z samples, i.e., $\log(L_{\rm FIR}) = 0.62\log(L_{\rm bol}) + 3.9$, and the dashed line shows the fit to the submillimeter or millimeter detected sources in all high-z samples and the local ULIRGs, $\log(L_{\rm FIR}) = 0.45\log(L_{\rm bol}) + 6.6$.

0.62 might suggest contributions from both host galaxy star formation and AGN power to the FIR emission (Beelen 2004; Netzer et al. 2007; Hao et al. 2005, 2008; Wang et al. 2008a; Serjeant & Hatziminaoglou 2009; Lutz et al. 2010).

The MAMBO-250 GHz observations at sub-mJy sensitivity have detected the most FIR luminous objects among the $z \sim 6$ quasars (Bertoldi et al. 2003a; Petric et al. 2003; Wang et al. 2007, 2008; this work). Most of these objects follow the shallower luminosity correlation trend of the local IR quasars and the (sub)mm-detected quasars at $z \sim 2$ to 5. In particular, the five MAMBO-detected $z \sim 6$ quasars with $m_{1450} \geqslant 20.2$ (Willott et al. 2007; Wang et al. 2008a; this work) overlap with the high luminosity end of the IR quasars. This may suggest a starburst-dominant FIR emission in these most FIR luminous quasars at $z \sim 6$, similar to that found in the local IR quasars. A fit to all the (sub)mm detections in the high-z quasar sample and the local IR quasars gives a relationship of

$$\log\left(\frac{L_{\rm FIR}}{L_\odot}\right) = (0.45 \pm 0.03)\log\left(\frac{L_{\rm bol}}{L_\odot}\right) + (6.62 \pm 0.39). \quad (2)$$

5. DISCUSSION: STAR FORMATION IN THE MAMBO-DETECTED FAINT $z \sim 6$ QUASARS

Strong FIR dust continuum emission has been detected in the host galaxies of $\gtrsim$1/4 of the faint $z \sim 6$ quasars ($m_{1450} \geqslant 20.2$; Willott et al. 2007; Wang et al. 2008a, 2010; this work). The dust continuum and molecular CO detections reveal a few $\times 10^8\, M_\odot$ of FIR-emitting warm dust and $10^{10}\, M_\odot$ of molecular gas in the host galaxies of these faint quasars, which are comparable to the typical values found with the millimeter-detected optically bright SDSS $z \sim 6$ quasars. The dust formation process associated with the evolution of massive stars on time scales $\lesssim$1 Gyr has been discussed widely since the discovery of $4 \times 10^8\, M_\odot$ of dust in one of the most luminous/massive $z \sim 6$ quasars, J1148+5251 (Beelen et al. 2006; Morgan & Edmunds 2003; Maiolino et al. 2004; Dwek et al. 2007). The detections of comparable amounts of dust in these faint $z \sim 6$ quasars may suggest similar fast dust formation mechanism in their host galaxies. Their FIR luminosities estimated from the

millimeter measurements are 3–5 $\times 10^{12}\ L_{\odot}$, falling on the FIR-to-AGN luminosity trend defined by the local IR quasars and the FIR luminous quasars at $z \sim 2$–5 (Section 4.2). The lower limit of their average FIR-to-radio emission ratio of $q > 1.6$ derived with the 250 GHz and 1.4 GHz measurements is within the typical range of $1.6 < q < 3.0$ in star-forming galaxies (Section 4.1).

All these results suggest significant star formation in the millimeter-detected optically faint quasars at the highest redshift. Conservatively assuming that 50% of the FIR emission is powered by host galaxy star formation, the average star formation rate (SFR) of the five millimeter-detected $m_{1450} \geqslant 20.2$ quasars is about 560 $M_{\odot}\ \mathrm{yr}^{-1}$ (Kennicutt 1998). Three of them have been detected in molecular CO (6–5) line emission (Wang et al. 2010; this work) and the ratios between FIR and CO luminosities are 220–370 $L_{\odot}\,\mathrm{K\,km\,s^{-1}\,pc^{2}}$, which is within the typical range found with the submillimeter galaxies and CO-detected quasars at lower redshifts (Solomon & Vanden Bout 2005; Greve et al. 2005). This result suggests a high star formation efficiency in these CO-detected faint $z \sim 6$ quasars, similar to that of the extreme starburst systems (Solomon & Vanden Bout 2005). Additionally, if the MAMBO-detected faint $z \sim 6$ quasars are indeed less massive SMBH systems accreting at their Eddington limit, the higher $\langle L_{\mathrm{FIR}}\rangle/\langle L_{1450}\rangle$ found with these object (see Table 4) may suggest a higher ratio between SFR and SMBH accretion rate in these systems compared to the MAMBO detections among the optically bright $z \sim 6$ quasars. This may indicate that the stellar bulge grows faster than the central SMBH in these faint/less massive quasar-host systems at $z \sim 6$.

6. CONCLUSIONS

We present observations of millimeter and radio continuum and CO(6–5) line emission from the host galaxies of quasars at $z \sim 6$. The new observations complete our MAMBO dust continuum survey of all the UV/optically faint $z \sim 6$ quasars ($m_{1450} \geqslant 20.2$) discovered from SDSS. Combining with previous data, we calculate the average FIR and radio emission for a sample of 18 $z \sim 6$ quasars with $m_{1450} \geqslant 20.2$. The mean FIR-to-AGN UV luminosity ratio of this faint quasar sample is about two times higher than that of the bright $z \sim 6$ quasars ($m_{1450} < 20.2$). A fit to the average FIR and AGN bolometric luminosities of both the UV/optically faint and bright $z \sim 6$ quasars, and the average luminosities of samples of submillimeter/millimeter-observed quasars at $z \sim 2$ to 5, yields a relationship of $L_{\mathrm{FIR}} \sim {L_{\mathrm{bol}}}^{0.62}$. The millimeter observations have detected the most FIR luminous objects among these faint $z \sim 6$ quasars. The 250 GHz dust continuum detections in five of the 18 faint quasars and CO (6–5) line detections in three of them (see Tables 1 and 2) reveal dust masses of a few $10^{8}\ M_{\odot}$ and molecular gas masses of $10^{10}\ M_{\odot}$ in the quasar host galaxies, which are comparable to the dust and gas masses found in the bright $z \sim 6$ quasars (Beelen et al. 2006; Bertoldi et al. 2003b; Carilli et al. 2007; Wang et al. 2008b, 2010). Their FIR luminosities are estimated to be 2.6–5.5 $\times 10^{12}\ L_{\odot}$, and the FIR and AGN bolometric luminosities follow a shallower relationship of $L_{\mathrm{FIR}} \sim {L_{\mathrm{bol}}}^{0.45}$, in agreement with the starburst–AGN systems at lower redshifts. All these results suggest active star formation in the host galaxies of the millimeter-detected and UV/optically faint quasars at $z \sim 6$ with SFRs of a few hundred $M_{\odot}\ \mathrm{yr}^{-1}$. Moreover, the higher average FIR-to AGN UV luminosity ratios (Table 4) found with these objects and the shallow luminosity relationship suggest higher SFR-to-AGN accretion rate ratios than that of the more luminous/massive $z \sim 6$ quasars. Further high-resolution imaging of the dust and molecular gas components (e.g., with ALMA) in the quasar host galaxies will be critical to constrain the host galaxy dynamical mass, black hole–spheroidal-host-mass ratio, gas and star formation rate surface density of these objects.

This work is based on observations carried out with the Max Planck Millimeter Bolometer Array (MAMBO) on the IRAM 30 m telescope, the Plateau de Bure Interferometer, and the Very Large Array (NRAO). IRAM is supported by INSU/CNRS (France), MPG (Germany) and IGN (Spain). The National Radio Astronomy Observatory (NRAO) is a facility of the National Science Foundation operated under cooperative agreement by Associated Universities, Inc. We acknowledge support from the Max-Planck Society and the Alexander von Humboldt Foundation through the Max-Planck-Forschungspreis 2005. Dominik A. Riechers acknowledges support from NASA through Hubble Fellowship grant HST-HF-51235.01 awarded by the Space Telescope Science Institute, which is operated by the Association of Universities for Research in Astronomy, Inc., for NASA, under contract NAS 5-26555. M. A. Strauss thanks the support of NSF grant AST-0707266.

Facilities: IRAM:30m (MAMBO), VLA, IRAM: Interferometer

REFERENCES

Beelen, A. 2004, PhD thesis, Observatoire de Paris
Beelen, A., Cox, P., Benford, D. J., et al. 2006, ApJ, 642, 694
Bertoldi, F., Carilli, C. L., Cox, P., et al. 2003a, A&A, 406, L55
Bertoldi, F., Cox, P., Neri, R., et al. 2003b, A&A, 409, L47
Carilli, C. L., Bertoldi, F., Rupen, M. P., et al. 2001, ApJ, 555, 625
Carilli, C. L., Neri, R., Wang, R., et al. 2007, ApJ, 666, L9
Carilli, C. L., Walter, F., Bertoldi, F., et al. 2004, AJ, 128, 997
Condon, J. J. 1992, ARA&A, 30, 575
Cool, R. J., Kochanek, C. S., Eisenstein, D. J., et al. 2006, AJ, 132, 823
Downes, D., & Solomon, P. M. 1998, ApJ, 507, 615
Dwek, E., Galliano, F., & Jones, A. P. 2007, ApJ, 662, 927
Fan, X., Hennawi, J. F., Richards, G. T., et al. 2004, AJ, 128, 515
Fan, X., Narayanan, V. K., Lupton, R. H., et al. 2001, AJ, 122, 2833
Fan, X., Strauss, M. A., Richards, G. T., et al. 2006, AJ, 131, 1203
Fan, X., Strauss, M. A., Schneider, D. P., et al. 2003, AJ, 125, 1649
Fan, X., White, R. L., Davis, M., et al. 2000, AJ, 120, 1167
Fomalont, E. B., Kellermann, K. I., Cowie, L. L., et al. 2006, ApJS, 167, 103
Greve, T. R., Bertoldi, F., Smail, I., et al. 2005, MNRAS, 359, 1165
Guilloteau, S., & Lucas, R. 2000, in ASP Conf. Proc.. 217, Imaging at Radio through Submillimeter Wavelengths, ed. J. G. Mangum & S. J. E. Radford (San Francisco, CA: ASP), 299
Hao, C. N., Xia, X. Y., Mao, S., et al. 2005, ApJ, 625, 78
Hao, C. N., Xia, X. Y., Mao, S., Deng, Z. G., & Wu, H. 2008, Chin. J. Astron. Astrophys., 8, 1
Hildebrand, R. H. 1983, QJRAS, 24, 267
Isobe, T., Feigelson, E. D., Akritas, M. G., & Babu, G. J. 1990, ApJ, 364, 104
Jiang, L., Fan, X., Annis, J., et al. 2008, AJ, 135, 1057
Jiang, L., Fan, X., Bian, F., et al. 2009, AJ, 138, 305
Jiang, L., Fan, X., Vestergaard, M., et al. 2007, AJ, 134, 1150
Kellermann, K. I., Sramek, R., Schmidt, M., et al. 1989, AJ, 98, 1195
Kennicutt, R. C. 1998, ARA&A, 36, 189
Kreysa, E., Gemuend, H., Gromke, J., et al. 1998, SPIE, 3357, 319
Kurk, J. D., Walter, F., Fan, X., et al. 2007, ApJ, 669, 32
Kurk, J. D., Walter, F., Fan, X., et al. 2009, ApJ, 702, 833
Lutz, D., Mainieri, V., Rafferty, D., et al. 2010, ApJ, 712, 1287
Maiolino, R., Schneider, R., Oliva, E., et al. 2004, Nature, 431, 533
McGreer, I. D., Becker, R. H., Helfand, D. J., & White, R. L. 2006, ApJ, 652, 157
Momjian, E., Carilli, C. L., & McGreer, I. D. 2008, AJ, 136, 344
Morgan, H. L., & Edmunds, M. G. 2003, MNRAS, 343, 427
Mortlock, D. J., Patel, M., Warren, S. J., et al. 2009, A&A, 509, 97

Netzer, H., Lutz, D., Schweitzer, M., et al. 2007, ApJ, 666, 806
Omont, A., Beelen, A., Bertoldi, F., et al. 2003, A&A, 398, 857
Omont, A., Cox, P., Bertoldi, F., et al. 2001, A&A, 374, 371
Petric, A. O., Carilli, C. L., Bertoldi, F., et al. 2003, AJ, 126, 15
Priddey, R. S., Isaak, K. G., McMahon, R. G., & Omont, A. 2003a, MNRAS, 339, 1183
Priddey, R. S., Isaak, K. G., McMahon, R. G., Roboson, E. I., & Pearson, C. P. 2003b, MNRAS, 344, L74
Richards, G. T., Lacy, M., Storrie-Lombardi, L. J., et al. 2006, ApJS, 166, 470
Richards, G. T., Vanden Berk, D. E., Reichard, T. A., et al. 2002, AJ, 124, 1
Riechers, D. A., Walter, F., Bertoldi, F., et al. 2009, ApJ, 703, 1338
Riechers, D. A., Walter, F., Carilli, C. L., et al. 2006, ApJ, 650, 604
Seaquist, E. R., Ivison, R. J., & Hall, P. J. 1995, MNRAS, 276, 867
Serjeant, S., & Hatziminaoglou, E. 2009, MNRAS, 397, 265
Solomon, P. M., Downes, D., Radford, S. J. E., & Barrett, J. W. 1997, ApJ, 478, 144
Solomon, P. M., & Vanden Bout, P. A. 2005, ARA&A, 43, 677 (SV05)
Spergel, D. N., Bean, R., Doré, O., et al. 2007, ApJS, 170, 377
Venemans, B. P., McMahon, R. G., Warren, S. J., et al. 2007, MNRAS, 376, L76
Walter, F., Bertoldi, F., Carilli, C., et al. 2003, Nature, 424, 406
Walter, F., Carilli, C. L., Bertoldi, F., et al. 2004, ApJ, 615, L17
Walter, F., Riechers, D., Cox, P., et al. 2009, Nature, 457, 699
Wang, R., Carilli, C. L., Beelen, A., et al. 2007, AJ, 134, 617
Wang, R., Carilli, C. L., Wagg, J., et al. 2008a, ApJ, 687, 848
Wang, R., Carilli, C. L., Neri, R., et al. 2010, ApJ, 714, 699
Wang, R., Wagg, J., Carilli, C. L., et al. 2008b, AJ, 135, 1201
Wang, R., Wagg, J., Carilli, C. L., et al. 2011, ApJL, in press (arXiv:1105.4199)
Willott, C. J., Delorme, P., Omont, A., et al. 2007, AJ, 134, 2435
Willott, C. J., Delorme, P., Reylé, C., et al. 2009, AJ, 137, 3541
Willott, C. J., Delorme, P., Reylé, C., et al. 2010a, AJ, 139, 906
Willott, C. J., Albert, L., Arzoumanian, D., et al. 2010b, AJ, 140, 546
Yun, M. S., Reddy, N. A., & Condon, J. J. 2001, ApJ, 554, 803
Zheng, X. Z., Xia, X. Y., Mao, S., et al. 2002, AJ, 124, 18
Zylka, R. 1998, MOPSI Users Manual (Grenoble: IRAM)